View metadata, citation and similar papers at core.ac.uk

brought to you by CORE

provided by IUPUIScholarWorks

HHS Public Access

Author manuscript

Int J Radiat Oncol Biol Phys. Author manuscript; available in PMC 2019 November 15.

Published in final edited form as:

Int J Radiat Oncol Biol Phys. 2018 November 15; 102(4): 1265–1275. doi:10.1016/j.ijrobp.2018.05.049.

Modeling Patient-Specific Dose-Function Response for Enhanced Characterization of Personalized Functional Damage

Daniel Rocky Owen, BS[*], **Phillip S. Boonstra, PhD**[†], **Benjamin L. Viglianti, MD, PhD**[‡,‖], **James M. Balter, PhD**[*], **Matthew J. Schipper, PhD**[†], **William C. Jackson, MD**[*], **Issam El Naqa, PhD**[*], **Shruti Jolly, MD**[*], **Randall K. Ten Haken, PhD**[*], **Feng-Ming Spring Kong, MD, PhD**[§], and **Martha M. Matuszak, PhD**[*]

[*]Department of Radiation Oncology, University of Michigan, Ann Arbor, Michigan

[†]Department of Biostatistics, University of Michigan, Ann Arbor, Michigan

[‡]Department of Radiology, University of Michigan, Ann Arbor, Michigan

[§]Department of Radiation Oncology, Indiana University School of Medicine, Indianapolis, Indiana

[‖]Nuclear Medicine Service, Veterans Affairs, Ann Arbor, Michigan

Abstract

Purpose: Functional-guided radiation therapy (RT) plans have the potential to limit damage to normal tissue and reduce toxicity. Although functional imaging modalities have continued to improve, a limited understanding of the functional response to radiation and its application to personalized therapy has hindered clinical implementation. The purpose of this study was to retrospectively model the longitudinal, patient-specific dose-function response in non-small cell lung cancer patients treated with RT to better characterize the expected functional damage in future, unknown patients.

Methods and Materials: Perfusion single-photon emission computed tomography/computed tomography scans were obtained at baseline (n = 81), midtreatment (n = 74), 3 months post-treatment (n = 51), and 1 year post-treatment (n = 26) and retrospectively analyzed. Patients were treated with conventionally fractionated RT or stereotactic body RT. Normalized perfusion single-photon emission computed tomography voxel intensity was used as a surrogate for local lung function. A patient-specific logistic model was applied to each individual patient's dose-function response to characterize functional reduction at each imaging time point. Patient-specific model parameters were averaged to create a population-level logistic dose-response model.

Results: A significant longitudinal decrease in lung function was observed after RT by analyzing the voxelwise change in normalized perfusion intensity. Generated dose-function response models

Reprint requests to: Daniel Rocky Owen, BS, 519 W William St., Ann Arbor, MI 48104. Tel: (650)575-7959; rockyo@umich.edu.

Conflict of interest: P.S.B. and J.M.B. report grants from the National Institutes of Health during the conduct of the study. I.E.N. reports grants from the National Institutes of Health outside the submitted work. R.K.T.H. and M.M.M. report grants from the National Institutes of Health during the conduct of the study and nonfinancial support from Varian Medical Systems outside the submitted work. F-M. S.K. reports grants from the National Cancer Institute during the conduct of the study and grants and personal fees from Varian Medical Systems outside the submitted work.

Supplementary material for this article can be found at www.redjournal.org.

Author Manuscript

Author Manuscript

Author Manuscript

Author Manuscript

Author Manuscript Author Manuscript Author Manuscript Author Manuscript

represent the expected voxelwise reduction in function, and the associated uncertainty, for an unknown patient receiving conventionally fractionated RT or stereotactic body RT. Differential treatment responses based on the functional status of the voxel at baseline suggest that initially higher functioning voxels are damaged at a higher rate than lower functioning voxels.

Conclusions: This study modeled the patient-specific dose-function response in patients with non-small cell lung cancer during and after radiation treatment. The generated population-level dose-function response models were derived from individual patient assessment and have the potential to inform functional-guided treatment plans regarding the expected functional lung damage. This type of patient-specific modeling approach can be applied broadly to other functional response analyses to better capture intrapatient dependencies and characterize personalized functional damage.

Introduction

Functional-guided radiation therapy (RT) has long been hypothesized to improve patient outcome (1–8). By quantifying perfusion and ventilation in normal lung tissue, a patient's 3-dimensional functional lung distribution can be incorporated into treatment planning to personalize radiation exposure (9–12). This personalization of treatment is especially important in patients with non-small cell lung cancer (NSCLC), who are known to have comorbidities and functional lung defects that change during the course of fractionated RT (13–16). Recent clinical studies have shown significant differences between anatomic-and functional-guided radiation treatment plans using a variety of functional imaging modalities, such as single-photon emission computed tomography (SPECT) (17–20), 4-dimensional computed tomography (CT) (21–24), and hyperpolarized magnetic resonance imaging (25, 26). Although preliminary studies have predicted toxicity reduction using functional-guided RT (27, 28), further work is still required to explicitly understand normal-tissue dose-function response and its effect on radiation-induced lung toxicity (RILT) incidence.

Perfusion SPECT/CT imaging provides a quantitative measure of pulmonary function such that normalized intensities within each lung voxel are representative of local vascular concentrations (29, 30). In 1994, Boersma et al first proposed using a logistic model to describe dose-function response (30). Because of the observed high variation in patient-to-patient dose response, Marks et al used a voxel-weighted average to determine composite perfusion loss (31). These studies provided the foundation for longitudinal quantification of functional lung using SPECT/CT imaging (1, 2), and the basis of these methodologies has been applied extensively to characterize dose-function response for various treatments, time points, and regions of the lung (32–37). Yet, most normal-tissue complication probability models currently used to assess risk of RILT rely on volumetric dose metrics that do not account for the heterogeneous distribution of functional lung (38–42). Although dose-volume metrics are important determinants of RILT incidence, recent evidence suggests functional information can provide additional benefit in assessing and predicting treatment response (43, 44). Ideally, a patient's risk of developing toxicity could be predicted by quantifying the expected cumulative functional lung damage for a given radiation treatment plan. However, enhanced modeling methods are still needed to accurately characterize lung function response and to facilitate clinical implementation of personalized RT.

Author Manuscript Author Manuscript Author Manuscript Author Manuscript

The purpose of this study was to quantify the longitudinal dose-function response in patients with NSCLC treated with conventionally fractionated RT and stereotactic body RT (SBRT). A patient-specific modeling approach was applied to retrospectively characterize each patient's functional change, using perfusion SPECT/CT. Individual patient models were then used to derive a population-level model that best represents the expected dose-function response in a new patient. The model was further segmented by functional categorization at baseline to enhance the prediction of functional lung damage based on an individual's pretreatment condition.

Methods and Materials

Study population

A total of 81 patients with histologically verified NSCLC were enrolled in an institutional review board-approved study and retrospectively analyzed. Written informed consent was obtained from all patients. Patients were treated with conventionally fractionated 3-dimensional conformal RT, with (n = 47) or without (n = 13) concurrent chemotherapy, or with SBRT (n = 21). A summary of the patient, disease, and treatment characteristics of the cohort is presented in Table 1.

SPECT imaging

Perfusion SPECT images of the lung were obtained at 4 separate time points: (1) pre-treatment; (2) mid-treatment (Mid-Tx); (3) 3 months post-treatment (3Month Post-Tx); and (4) 1 year post-treatment (1Year Post-Tx). SPECT imaging was performed by using a dual-head SPECT/CT system (Symbia T6, Siemens Medical Solutions, Malvern, PA) with the patient immobilized in the supine treatment position using a standard thorax support device for reproducibility. Each patient was first scanned for pulmonary ventilation mapping by inhaling aerosolized ^{99m} Tc-diethylenetriaminepentaacetic acid from an 1850 MBq reservoir. Pulmonary perfusion was subsequently scanned after intravenous injection of 185 MBq of ^{99m}Tc-labeled macroaggregated albumin particles.

SPECT scans were obtained with a noncircular orbit over a 360° arc in 60 projections and 128 frames (19 s/frame, 3° increments, 128 pixels × 128 pixels, ~3. 5 mm × ~3.5 mm × 2 mm) by using the stop-and-shoot mode. The SPECT images were reconstructed by initially applying attenuation and scatter correction and subsequently implementing a 3-dimensional ordered subset expectation-maximization iterative reconstruction with resolution, scatter, and attenuation corrections.

CT-based simulation and treatment planning

Simulation CT scans were obtained for each patient, with patients in the supine position, before treatment. Data were accrued over a 6-year period (2007–2013). Early in the study period, patients were assessed for motion through analysis of inhale and exhale CT scans. As the study progressed, 4-dimensional CT was incorporated for motion assessment. Patients with extensive motion were prescribed breath-hold treatments, and all free-breathing patients were treated with an internal target volume approach. The Eclipse Analytical Anisotropic Algorithm (Varian Medical Systems, Palo Alto, CA) photon dose

Author Manuscript Author Manuscript Author Manuscript Author Manuscript

model was used to retrospectively calculate the delivered dose to each voxel in the CT matrix (512 pixels × 512 pixels, 0.98 mm × 0.98 mm × 3 mm). For each patient, the calculated dose in each normal lung voxel was then corrected to the nominal dose equivalent per 2 Gy fraction (EQD2) using the linear quadratic model with an α/β ratio of 2.5 Gy (45). Lung structures were contoured as part of treatment planning and edited according to a thoracic atlas (46). Normal lung tissue was defined as all voxels within the lungs excluding the gross tumor volume.

SPECT registration

SPECT scans were available for 81 patients at baseline, 75 at Mid-Tx, 52 at 3Month Post-Tx, and 28 at 1Year Post-Tx. For a given patient, each available SPECT scan was rigidly aligned to the treatment planning CT. Rigid registrations were manually reviewed for accuracy. After registration, each voxel within the normal lung tissue contained both a dose value and function value (ie, normalized perfusion SPECT intensity). As in previous studies, rigid registration was performed instead of deformable registration to avoid uncharacterized errors that may be caused by low spatial resolution and unmatched breathing states between the SPECT/CT and planning CT images.

Normalization

To account for varying absolute intensity in SPECT scans taken across different time points and patients, the raw intensity value in each voxel was normalized. Because minimal functional changes are expected in low-dose regions, the functional normalization constant was determined as the average intensity in the functioning region (ie, all voxels >10% of maximum intensity) of the contralateral lung that received less than 5 Gy. Normalized intensity signal in any voxel is a relative measure of the local perfusion compared with the average functional value in unaffected tissue.

Data processing

To reduce the well-documented effect of ^{99m}Tc aerosol-trapping artifacts in patients with obstructive airway disease (47, 48), any voxel with an intensity value greater than 3 standard deviations above the mean intensity of the high-functioning lung region (ie, all voxels >50% of maximum intensity) was excluded. On average, 0.3% of the perfusion voxels were excluded from the normal lung volume.

Dose-function response

In this study, normalized perfusion intensity was applied directly as a surrogate for local lung function. To characterize each patient's dose-function response over time, the normalized intensity in each voxel at the Mid-Tx, 3Month Post-Tx, and 1Year Post-Tx time points was compared to the normalized intensity in the same voxel at baseline:

$$\delta_{f,t,j,i} = f^{\mathbb{N}}_{i,t} - f^{\mathbb{N}}_{i,t=0} \quad (1)$$

Author Manuscript Author Manuscript Author Manuscript Author Manuscript

where $f^{\mathbb{N}}_{i,t=0}$ is the normalized functional intensity signal in the ith voxel at time point t = {0 = b*aseline*; 1 = *Mid - tx* ;2 = *3Month Post - tx*;3 = *1Year Post – tx*}. Dose bins of 5 Gy increments were used to tally the average functional change.

Patient-specific dose-function response modeling

To account for interdependencies within an individual patient's dose-function response, the 3-parameter logistic model described by Scheenstra et al (36) was expanded to allow for a patient-specific asymptote (α_j, maximum possible reduction) and midpoint (μ_j; ie, the dose at which 50% of the maximum reduction occurs). This is a common analytic approach for correlated data and is also called a nonlinear mixed effects model, which refers to the mixture of population-and patient-specific parameters (49). As such, the reduction in baseline intensity for patient j at dose bin i is modeled as

$$\text{Patient}-\text{specific logistic model: } \frac{\alpha_j}{1+e^{-\left(\mu_j-d_i\right)/\gamma}} \quad (2)$$

A non-patient-specific (ie, population-averaged) inverse of the dose-effect slope at midpoint (γ) was set for all patients because of instability in fitting a patient-specific slope parameter. Using Equation 2, each patient's average dose-function response data points were fit to obtain the patient-specific model parameters. Because the patient-specific effects are assumed to be centered around global means, the population-average midpoint (μ) and maximum possible reduction (α) were calculated by averaging the patient-specific model parameters obtained from the cohort. As such, the population-level model takes the following form:

$$\text{Population}-\text{level logistic model: } \frac{\alpha}{1+e^{-\left(\mu-d_i\right)/\gamma}} \quad (3)$$

where d_i is the dose at the center of dose bin i. By allowing each patient's dose-function response to be represented through a logistic function, the derived population-averaged logistic model better represents a patient's coherent functional reduction over all dose bins.

The patient-specific logistic function was further modified to characterize dose response stratified by baseline intensity, as shown:

$$\text{Stratified patient}-\text{specific model: } \frac{\alpha_j+\omega_k}{1+e^{-\left(\mu_j-d_i\right)/\gamma}} \quad (4)$$

where k denotes the baseline intensity group, and $\alpha_j + \omega_k$denotes the patient-specific asymptote for voxels in group k. For identifiability, ω_4 was set to zero. The model shown in Equation 3 was used to describe the population-level response in each functional category.

Author Manuscript Author Manuscript Author Manuscript Author Manuscript

Voxels were grouped with respect to baseline perfusion. Specifically, the groups included all voxels with baseline intensity, expressed as a percent of the maximum normal-tissue intensity, in the following ranges:

$$\{k = 1{:}10\%\ to\ 30\%\ of\ baseline\ max;\ k = 2{:}30\%\ to\ 50\%;\ k = 3{:}50\%\ to\ 75\%;\ k = 4\ {:>}\ 75\%\}$$

Voxels below 10% of the maximum intensity were excluded from the analysis on the basis of the low number of counts. The 4 functional categories, which roughly correspond to quartiles, were chosen before performance of the statistical analysis.

The standard deviation in the reduction of function from baseline was allowed to vary with the number of voxels:

$$\text{Standard deviation: } \sigma\left(m_{ij}\right)^{\lambda} \quad (5)$$

where m_{ij} is the number of voxels in dose bin i for patient j, σ is a scale parameter that describes the deviation between the patient-specific parameters and their population-level means, and λ modifies the deviation based on the number of voxels in that dose bin. Typically λ is negative, which corresponds to a reduction in variance with an increasing number of voxels. These models were fit using the *nlme* package in R (50).

Results

Voxelwise reduction in normalized perfusion intensity was modeled using a patient-specific logistic function. Functional reduction was measured and modeled as the decrease in normalized perfusion intensity, meaning a $\delta_{f;t;j;i}$ of −0.5 signifies a reduction of +0.5 normalized perfusion intensity units in that voxel. The presented models are graphically represented accordingly. For each patient, a normalized intensity of 1.0 signifies the average perfusion intensity of functioning voxels in the low-dose region of the contralateral lung. The population-level model parameters and standard deviations describing dose-perfusion response for the conventional RT and SBRT cohorts at each imaging time point are listed in Tables 2 and 3.

Dose-perfusion response for well-perfused voxels

Only well-perfused voxels were considered for the patient-specific and population-level dose-response curves shown in Fig. 1. The color data points represent the average functional change in that dose bin for each patient. Each individual patient's data points are coherently modeled, as shown by the color-matched, shaded lines, using the logistic function shown in Equation 2. The patient-specific models are used to develop the bolded population-level dose-function response curves, as described by Equation 3. The population-level model fits and the associated uncertainty are explicitly tabulated in Table 2 and graphically shown in Fig. 2A. The shaded 95% confidence intervals are a function of both the spread in the distribution of patientspecific responses and the number of voxels contributing to the data, as shown in Equation 5. A significant longitudinal increase in perfusion reduction is clearly

Author Manuscript Author Manuscript Author Manuscript Author Manuscript

observed, suggesting that lung function continues to degrade up to 1 year post-treatment. The maximal possible reduction asymptote ranged from approximately 30 to 60 Gy (EQD2), depending on the time point and treatment type. The patientspecific population-level models were compared with the population-level voxel-weighted average data points and non-patient-specific logistic models (ie, simply fitting Equation 3 to the population-averaged data points), as shown in Fig. 2B.

Stratified dose-perfusion response for normalized baseline intensity >10% of the maximum

The patient-specific voxelwise reduction in normalized perfusion intensity with respect to planned dose was modeled for each stratified baseline intensity level using Equation 4. The population-level models can be interpreted as a prediction for voxelwise functional maximal reduction in each voxel group is longitudinally increasing (ie, $\omega_1 < \omega_2 < \omega_3 < \omega_4 = 0$), and at the 3- and 12-month post-treatment time points, the confidence intervals for each parameter are nonoverlapping. This trend between perfusion reduction and baseline function in both cohorts suggests that higher functioning voxels at baseline are damaged at a greater rate than lower functioning voxels.

Discussion

This study quantified the voxelwise reduction in perfusion during and after radiation treatment by measuring the longitudinal change in normalized SPECT intensity, similar to methods in previous works. However, this analysis aimed to enhance the characterization of personalized functional changes by applying a patient-specific modeling approach that explicitly accounts for interdependencies within an individual patient's dose-function response. Using this methodology, population-averaged dose-function response curves and their uncertainties were calculated for patients with NSCLC undergoing conventional RT and SBRT.

From age to chemotherapy to comorbidities, many patient-, treatment-, and disease-related factors explicitly affect an individual's dose-function response (51–53). Each patient has a unique signature that inherently creates a distinct treatment response curve. As such, the voxels and the corresponding dose effect from one patient are more closely related to each other than to voxels from a different patient. Although the dose effect has classically been modeled by fitting population-averaged data points, it is proposed that a patient-specific model can more accurately describe the coherent dose-function response in an individual patient.

Logistic models have classically been used to describe dose-effect relations for cell survival. Boersma et al first proposed using the logistic model to describe changes in vascular subunits within the lung (31). Scheenstra et al recently showed that local functional changes in patients undergoing SBRT were best represented through a logistic model driven by 3 parameters: *(1)* maximal reduction effect (asymptote); *(2)* dose to obtain 50% of maximal effect (midpoint); and *(3)* slope of the linear dose effect (36). However, because a patient's signature effects the dose-function response over all dose bins, there is an inherent correlation among data points contributed by each patient. As a consequence of Jensen's inequality, averaging each dose bin across patients would introduce bias in the resulting

Author Manuscript Author Manuscript Author Manuscript Author Manuscript

estimated population-average curve (54). Therefore, a mixed-effects nonlinear regression model was used in this analysis to allow for a patient-specific maximal effect and midpoint dose, as shown in Equation 2. With this approach, each patient's dose-perfusion response assumed a unique form, and population-level trends were derived, as shown in Fig. 1. With application of a logistic function to each individual patient's data (as opposed to averaging each dose bin separately), the derived population-level model will better estimate the dose-function response for a future, unknown patient.

Only minimal reductions in the high-dose regions were observed during treatment, whereas increasing longitudinal reductions occurred in these same areas after treatment. Furthermore, both patients undergoing conventional RT and those receiving SBRT consistently reached an asymptote in functional reduction near the target dose, suggesting that the maximal reduction effect occurs at a lower dose in conventionally fractionated RT. Although nearly all patients exhibit perfusion reduction at 3Month Post-Tx, 3 patients in both the conventional RT and SBRT cohorts exhibit markedly better response at 1Year Post-Tx than the rest of their cohort. This suggests a recovery pathway and illustrates the need for patient-specific modeling.

Random effects were assumed to vary around population-level global means. Standard deviations were calculated to account for both the deviation from the mean and the statistical uncertainty associated with each data point. Therefore, the 95% confidence intervals represent the bounds of measured dose response for the conventional RT and SBRT cohorts. Analogously, these intervals can be interpreted as the uncertainty in predicting the voxelwise reduction in function from an unknown patient given the planned dose.

Previous works have mostly focused on analyzing functional response in well-perfused and well-ventilated regions. This focus stems from the idea that limiting dose to functioning lung can reduce toxicity by maintaining a patient's functional reserve. However, the well-perfused regions have not been consistently defined and only consist of a small portion of the lung receiving a high dose. This study modeled the well-perfused dose response for comparison with previous modeling techniques, as shown in Fig. 2B. However, this is the first study to differentially characterize dose-function response-based on pretreatment functional status-across all functioning voxels. Although deviations from the population-level models are observed, the consistent differential treatment response suggests that initially higher functioning voxels exhibit a higher rate of perfusion loss, as shown in Fig. 3. Functional categorizations were chosen based on guidance from previous work (20, 33). Furthermore, the ranges were kept broad to ensure sufficient normal lung volume and limited statistical uncertainty in each category. However, because these categorizations were arbitrarily selected to represent functional capabilities, the bins may distinguish between regions that are not meaningfully different in their ability to exchange gas. Our results suggest that the voxelwise reduction in perfusion is a nonlinear function of baseline perfusion, in addition to being a nonlinear function of dose, which makes numerical fitting of this model substantially more difficult.

The amount of reperfusion has been shown to be directly proportional to perfusion deficiency (33), suggesting that perfusion reduction in initially poorly functioning regions is

Author Manuscript Author Manuscript Author Manuscript Author Manuscript

diminished by a reperfusion effect that is inversely proportional to baseline intensity. The response was quantified in all functioning voxels because it is hypothesized that any portion of lung that is functioning at baseline can consequently become damaged and contribute to the loss of functional reserve. Future studies aim to further investigate the reperfusion effect and alternatively model the potential for functional improvement.

Although SPECT/CT is generally considered the gold standard for functional lung imaging, challenges regarding limited spatial resolution and presence of artifacts have been well documented. Because each frame of the SPECT image is acquired over a time period that typically encompasses several cardiac and breathing cycles, physiological motion will lead to spatial blurring of the signals. Although this may introduce errors in individual voxel intensities, the large binning of voxels reduced the impact of decreased spatial resolution. Average functional change was tallied within 5 Gy isodose volumes (ie, dose bins) such that numerous voxels contribute within each region. Although the use of rigid registration for functional image characterization can result in uncertainties, especially in areas of large motion and deformation, deformable image registration has typically not been applied to SPECT imaging because of low spatial resolution. Future studies using SPECT images may be improved by adjusting the acquisition parameters to better match the breathing states between the SPECT/CT and the planning CT image.

In many functional imaging modalities, such as SPECT/ CT, normalization is required to quantitatively analyze longitudinal change. Most prior studies analyzing perfusion changes using SPECT/CT have normalized intensities using the average value of the functioning voxels in the low-dose region of the contralateral lung (31, 34, 35). Although the specific definition of the low-dose region has varied, the technique is generally well accepted because minimal functional changes are expected in voxels receiving a low dose. We have yet to apply a patientspecific modeling approach to the contralateral lung, but this assumption was supported by the finding that the population-averaged functional change in the contralateral lung did not decrease significantly below 15 Gy, as shown in Fig. E1 (available online at www.redjournal.org).

Because these clinical data were gathered between 2007 and 2013, patients were treated with a conventionally fractioned 3-dimensional conformal RT approach instead of the modern intensity modulated RT techniques currently used in the clinic. Many of these patients who received 3-dimensional conformal treatment would now be treated with volumetric modulated arc therapy, which would further change the dose-volume histogram profile. In an attempt to standardize the radiation effect between the treatment fractionation schemes, all doses were converted to EQD2 dose values. Furthermore, although some patient falloff occurred at the 3- and 12-month time points, we would not expect this loss of data to depend on the patient’s unobserved voxelwise dose-response curve; therefore, it should not cause bias in our estimated regression coefficients.

By characterizing the patient-specific dose-function response in all baseline functioning voxels, this work provides specific population-level estimates for the expected voxelwise reduction in perfusion at Mid-Tx, 3Month Post-Tx, and 1Year Post-Tx. These models allow for enhanced prediction of personalized functional damage by developing the population-

Author Manuscript Author Manuscript Author Manuscript Author Manuscript

level response through individual patient assessment and by segmenting the expected functional reduction based on a patient's pre-treatment functional status. In theory, by applying the generated doseresponse incidence models, the cumulative functional lung damage for an unknown patient could be predicted and used to support functional-guided RT plans by weighting voxels based on their risk of functional damage.

Conclusions

A patient-specific modeling approach was applied to quantify the dose-function response using perfusion SPECT/CT images in patients with NSCLC undergoing conventional RT and SBRT. By deriving functional response from patient-specific assessment, the population-level models presented in this analysis can be used to better predict functional lung damage in an unknown patient. Differential treatment responses were observed based on the functional status of the voxel at baseline, suggesting that the highest functioning voxels are damaged at the highest rate. Although further refinement is required to implement personalized predictions of functional damage in the clinic, this work provides a simple methodology, applicable to any functional imaging modality, to more accurately model dose-function response.

Supplementary Material

Refer to Web version on PubMed Central for supplementary material.

Acknowledgment

We thank Kirk Frey, MD, PhD, and colleagues in the Department of Radiology at the University of Michigan for their support in obtaining the protocol single-photon emission computed tomography/computed tomography scans used in this work.

This study has been supported in part by the National Institutes of Health (grant nos. R01-CA142840, P30-CA046592, and P01-CA059872).

References

1. Marks LB, Spencer DP, Bentel GC, et al. The utility of SPECT lung perfusion scans in minimizing and assessing the physiologic consequences of thoracic irradiation. Int J Radiat Oncol Biol Phys 1993;26: 659–668. [PubMed: 8330998]
2. Boersma LJ, Damena EMF, De Boera RW, et al. A new method to determine dose-effect relations for local lung-function changes using correlated SPECT and CT data. Radiother Oncol 1993;29:110–116. [PubMed: 8310136]
3. Marks LB, Spencer DP, Sherouse GW, et al. The role of three dimensional functional lung imaging in radiation treatment planning: The functional dose-volume histogram. Int J Radiat Oncol Biol Phys 1995;33:65–75. [PubMed: 7642433]
4. Boersmaa LJ, Damena EMF, De Boera RW, et al. Estimation of overall pulmonary function after irradiation using dose-effect relations for local functional injury. Radiother Oncol 1995;36:15–23. [PubMed: 8525021]
5. Seppenwoolde Y, Engelsman M, De Jaeger K, et al. Optimizing radiation treatment plans for lung cancer using lung perfusion information. Radiother Oncol 2002;63:165–177. [PubMed: 12063006]
6. Mcguire SM, Zhou S, Marks LB, et al. A methodology for using SPECT to reduce intensity-modulated radiation therapy (IMRT) dose to functioning lung. Int J Radiat Oncol Biol Phys 2006;66:1543–1552. [PubMed: 17126212]

Author Manuscript Author Manuscript Author Manuscript Author Manuscript

7. Shioyama Y, Jang SY, Liu HH, et al. Preserving functional lung using perfusion imaging and intensity-modulated radiation therapy for advanced-stage non-small cell lung cancer. Int J Radiat Oncol Bio Phys 2007;68:1349–1358. [PubMed: 17446001]
8. Wang D, Li B, Wang Z, et al. Functional dose-volume histograms for predicting radiation pneumonitis in locally advanced non-small cell lung cancer treated with late-course accelerated hyperfractionated radiotherapy. Exp Ther Med 2011;2:1017–1022. [PubMed: 22977614]
9. Marks LB, Sherouse GW, Munley MT, et al. Incorporation of functional status into dose-volume analysis. Med Phys 1999;26:196–199. [PubMed: 10076973]
10. Yaremko BP, Guerrero TM, Noyola-Martinez J, et al. Reduction of normal lung irradiation in locally advanced non-small cell lung cancer patients using ventilation images for functional avoidance. Int J Radiat Oncol Bio Phys 2007;68:562–571. [PubMed: 17398028]
11. St-hilaire J, Lavoie C, Dagnault A, et al. Functional avoidance of lung in plan optimization with an aperture-based inverse planning system. Radiother Oncol 2011;100:390–395. [PubMed: 21963286]
12. Yamamoto T, Kabus S, von Berg J, et al. Impact of four-dimensional computed tomography pulmonary ventilation imaging-based functional avoidance for lung cancer radiotherapy. Int J Radiat Oncol Bio Phys 2011;79:279–288. [PubMed: 20646852]
13. Janssen-Heijnen MLG, Schipper RM, Razenberg PPA, et al. Prevalence of co-morbidity in lung cancer patients and its relationship with treatment: A population-based study. Lung Cancer 1998;21:105–113. [PubMed: 9829544]
14. Durham AL, Adcock IM. The relationship between COPD and lung cancer. Lung Cancer 2015;90:121–127. [PubMed: 26363803]
15. Vinogradskiy Y, Schubert L, Diot Q, et al. Regional lung function profiles of stage I and III lung cancer patients: An evaluation for functional avoidance radiation therapy. Int J Radiat Oncol Bio Phys 2016;95:1273–1280. [PubMed: 27354134]
16. Meng X, Frey K, Matuszak M, et al. Changes in functional lung regions during the course of radiation therapy and their potential impact on lung dosimetry for non-small cell lung cancer. Int J Radiat Oncol Bio Phys 2014;89:145–151. [PubMed: 24725697]
17. Lavrenkov K, Christian JA, Partridge M, et al. A potential to reduce pulmonary toxicity: The use of perfusion SPECT with IMRT for functional lung avoidance in radiotherapy of non-small cell lung cancer. Radiother Oncol 2007;83:156–162. [PubMed: 17493699]
18. Munawar I, Yaremko BP, Craig J, et al. Intensity modulated radiotherapy of non-small-cell lung cancer incorporating SPECT ventilation imaging. Med Phys 2010;37:1863–1872. [PubMed: 20443508]
19. Liss AL, Marsh RB, Kapadia NS, et al. Decreased lung perfusion after breast/chest wall irradiation: Quantitative results from a prospective clinical trial. Int J Radiat Oncol Bio Phys 2017; 97:296–302. [PubMed: 27986344]
20. Lee E, Zeng J, Miyaoka RS, et al. Functional lung avoidance and response-adaptive escalation (FLARE) RT: Multimodality plan dosimetry of a precision radiation oncology strategy. Med Phys 2017; 44:3418–3429. [PubMed: 28453861]
21. Huang T-C, Hsiao C-Y, Chien C-R, et al. IMRT treatment plans and functional planning with functional lung imaging from 4D-CT for thoracic cancer patients. Radiat Oncol 2013;8:1–10. [PubMed: 23280007]
22. Yamamoto T, Kabus S, Bal M, et al. The first patient treatment of computed tomography ventilation functional image-guided radiotherapy for lung cancer. Radiother Oncol 2016;118:227–231. [PubMed: 26687903]
23. Faught AM, Yamamoto T, Castillo R, et al. Evaluating which dosefunction metrics are most critical for functional-guided radiation therapy. Int J Radiat Oncol Bio Phys 2017;99:202–209. [PubMed: 28816147]
24. Waxweiler T, Schubert L, Diot Q, et al. A complete 4DCT-ventilation functional avoidance virtual trial: Developing strategies for prospective clinical trials. J Appl Clin Med Phys 2017;18:144–152.
25. Ireland RH, Bragg CM, Mcjury M, et al. Feasibility of image registration and intensity-modulated radiotherapy planning with hyperpolarized helium-3 magnetic resonance imaging for non-smallcell lung cancer. Int J Radiat Oncol Bio Phys 2007;68:273–281. [PubMed: 17448880]

Author Manuscript Author Manuscript Author Manuscript Author Manuscript

26. Bates EL, Bragg CM, Wild JM, et al. Functional image-based radiotherapy planning for non-small cell lung cancer: A simulation study. Radiother Oncol 2009;93:32–36. [PubMed: 19552978]
27. Farr KP, Kramer S, Khalil AA, et al. Role of perfusion SPECT in prediction and measurement of pulmonary complications after radiotherapy for lung cancer. Eur J Nucl Med Mol Imaging 2015;42: 1315–1324. [PubMed: 25862455]
28. Faught AM, Miyasaka Y, Kadoya N, et al. Evaluating the toxicity reduction with computed tomographic ventilation functional avoidance radiation therapy. Int J Radiat Oncol Bio Phys 2017;99:325333.
29. Damen EMF, Muller SH, Boersma LJ, et al. Quantifying local lung perfusion and ventilation using correlated SPECT and CT data. J Nucl Med 1994;35:784–792. [PubMed: 8176459]
30. Boersma LJ, Damen EMF, De Boer RW, et al. Dose-effect relations for local functional and structural changes of the lung after irradiation for malignant lymphoma. Radiother Oncol 1994;32: 201–209. [PubMed: 7816939]
31. Marks LB, Munley MT, Spencer DP, et al. Quantification of radiation-induced regional lung injury with perfusion imaging. Int J Radiat Oncol Bio Phys 1997;38:399–409. [PubMed: 9226329]
32. Boersma LJ, Damen EM, de Boer RW, et al. Recovery of overall and local lung function loss 18 months after irradiation for malignant lymphoma. J Clin Oncol 1996;14:1431–1441. [PubMed: 8622056]
33. Seppenwoolde Y, Muller SH, Theuws JCM, et al. Radiation doseeffect relations and local recovery in perfusion for patients with nonesmall-cell lung cancer. Int J Radiat Oncol Bio Phys 2000;47: 681–690. [PubMed: 10837952]
34. Woel RT, Munley MT, Hollis D, et al. The time course of radiation therapy-induced reductions in regional perfusion: A prospective study with ˃5 years of follow-up. Int J Radiat Oncol Bio Phys 2002; 52:58–67. [PubMed: 11777622]
35. Zhang J, Ma J, Zhou S, et al. Radiation-induced reductions in regional lung perfusion: 0.1–12 year data from a prospective clinical study. Int J Radiat Oncol Bio Phys 2010;76:425–432. [PubMed: 19632063]
36. Scheenstra AEH, Rossi MMG, Belderbos JSA, et al. Local doseeffect relations for lung perfusion post stereotactic body radiotherapy. Radiother Oncol 2013;107:398–402. [PubMed: 23623727]
37. Farr KP, Møller DS, Khalil AA, et al. Loss of lung function after chemo-radiotherapy for NSCLC measured by perfusion SPECT/CT: Correlation with radiation dose and clinical morbidity. Acta Oncol 2015;54:1350–1354. [PubMed: 26203930]
38. Emami B, Lyman J, Brown A, et al. Tolerance of normal tissue to therapeutic irradiation. Int J Radiat Oncol Bio Phys 1991;21:109–122. [PubMed: 2032882]
39. Kim TH, Cho KH, Pyo HR, et al. Dose-volumetric parameters for predicting severe radiation pneumonitis after three-dimensional conformal radiation therapy for lung cancer. Radiology 2005;235:208–215. [PubMed: 15703313]
40. Marks LB, Bentzen SM, Deasy JO, et al. Radiation dose-volume effects in the lung. Int J Radiat Oncol Bio Phys 2010;76:70–76.
41. Marks LB, Yorke ED, Jackson A, et al. Use of normal tissue complication probability models in the clinic. Int J Radiat Oncol Bio Phys 2010;76:10–19.
42. Rodrigues G, Lock M, D'Souza D, et al. Prediction of radiation pneumonitis by doseevolume histogram parameters in lung cancerda systematic review. Radiother Oncol 2004;71:127–138. [PubMed: 15110445]
43. Farr KP, Kallehauge JF, Møller DS, et al. Inclusion of functional information from perfusion SPECT improves predictive value of dose-volume parameters in lung toxicity outcome after radiotherapyfor non-small cell lung cancer: A prospective study. Radiother Onco*l* 2015;117:9–16. [PubMed: 26303012]
44. Kimura T, Doi Y, Nakashima T, et al. Combined ventilation and perfusion imaging correlates with the dosimetric parameters of radiation pneumonitis in radiation therapy planning for lung cancer. Int J Radiat Oncol Bio Phys 2015;93:778–787. [PubMed: 26530746]
45. Li AX, Alber M, Deasy JO, et al. The use and QA of biologically related models for treatment planning: Short report of the TG-166 of the therapy physics committee of the AAPM. Med Phys 2012;39: 1386–1409. [PubMed: 22380372]

Author Manuscript Author Manuscript Author Manuscript Author Manuscript

46. Kong F-M, Ritter T, Quint DJ, et al. Consideration of dose limits for organs at risk of thoracic radiotherapy: Atlas for lung, proximal bronchial tree, esophagus, spinal cord, ribs, and brachial plexus. Int J Radiat Oncol Bio Phys 2011;81:1442–1457. [PubMed: 20934273]
47. Schembri GP, Roach PJ, Bailey DL, et al. Artifacts and anatomical variants affecting ventilation and perfusion lung imaging. Semin Nucl Med 2015;45:373–391. [PubMed: 26278851]
48. Bajc M, Neilly B, Miniati M, et al. Methodology for ventilation/perfusion SPECT. Semin Nucl Med 2010;40:415–425. [PubMed: 20920632]
49. Davidian M, Giltinan DM. Nonlinear models for repeated measurements: An overview and update. J Agric Biol Environ Stat 2003;8: 387–419.
50. Pinheiro J, Bates D, DebRoy S, et al. nlme: Linear and Nonlinear Mixed Effects Models; 2017 Available at: https://CRAN.R-project.org/package=nlme. Accessed October 15, 2017.
51. Fan M, Marks LB, Hollis D, et al. Can we predict radiation-induced changes in pulmonary function based on the sum of predicted regional dysfunction? J Clin Oncol 2001;19:543–550. [PubMed: 11208849]
52. Jin JY, Kong FM, Chetty IJ, et al. Impact of fraction size on lung radiation toxicity: Hypofractionation may be beneficial in dose escalation of radiotherapy for lung cancers. Int J Radiat Oncol Bio Phys 2010;76:782–788. [PubMed: 19577855]
53. Rajan Radha R, Chandrasekharan G. Pulmonary injury associated with radiation therapy e Assessment, complications and therapeutic targets. Biomed Pharmacother 2017;89:1092–1104. [PubMed: 28298070]
54. Jensen JLWV. Sur les fonctions convexes et les ine´galite´s entre les valeurs moyennes. Acta Math 1906;30:175–193.

Author Manuscript Author Manuscript Author Manuscript Author Manuscript

Summary

By quantifying the heterogeneous distribution of lung function prior to treatment, personalized radiation therapies have the potential to limit functional damage and reduce toxicity. However, a limited understanding of the normal-tissue response to radiation has hindered the incorporation of functional information in treatment planning. This study applied a patient-specific modeling approach to enhance characterization of the dose-function response in non-small cell lung cancer patients treated with conventionally fractionated radiation therapy and stereotactic body radiation therapy. In addition, the dose-function response was further stratified by baseline intensity, suggesting that initially well-perfused voxels are damaged at the highest rate.

Author Manuscript Author Manuscript Author Manuscript Author Manuscript

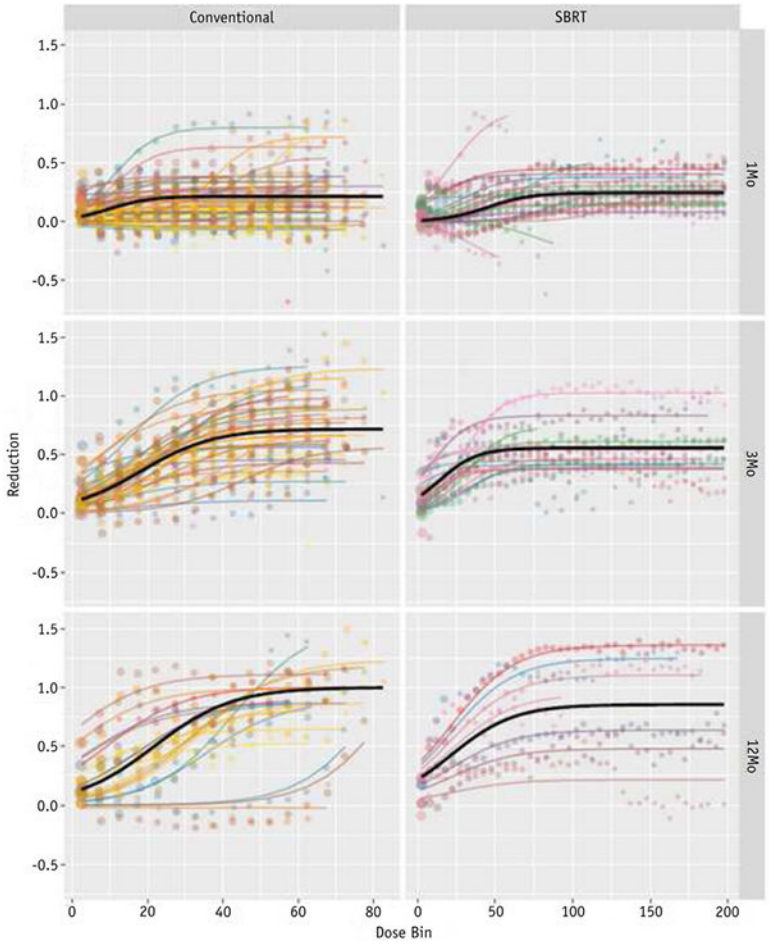

Fig. 1.

Individual patient dose-response bin averages (colored points) and patient-specific model fits (colored lines) overlaid with the population-level model fit (solid) for initially well-perfused voxels. *Abbreviations*: Conventional Z conventional radiation therapy; SBRT Z stereotactic body radiation therapy. (A color version of this figure is available at www.redjournal.org.)

Author Manuscript Author Manuscript Author Manuscript Author Manuscript

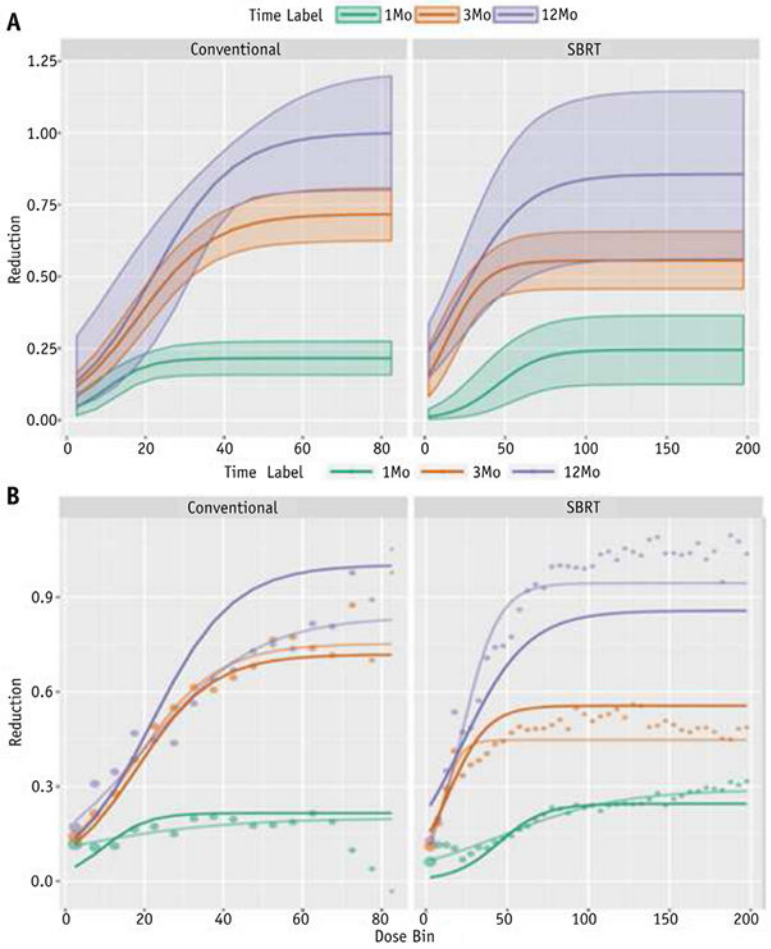

Fig. 2.

(A) Dose-perfusion response at mid-treatment (Mid-Tx) (green), 3 months post-treatment (3Month Post-Tx) (red), and 1 year post-treatment (1Year Post-Tx) (purple), fit using a patient-specific logistic model. The 95% confidence intervals are represented by the shaded region. (B) Patient-specific logistic model fits (solid lines) compared with the voxel-weighted average data (points) and non-patient-specific logistic model fits (shaded lines). *Abbreviations*: Conventional Z conventional radiation therapy; SBRT Z stereotactic body radiation therapy. (A color version of this figure is available at www.redjournal.org.)

Author Manuscript Author Manuscript Author Manuscript Author Manuscript

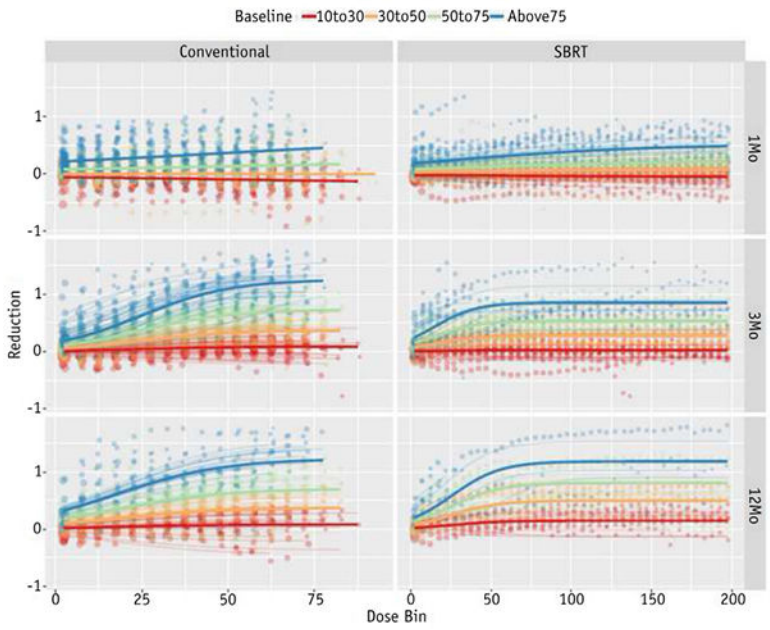

Fig. 3.

Stratified dose-perfusion response for voxels in each normalized baseline intensity level: 10% to 30% (red), 30% to 50% (orange), 50% to 75% (green), and >75% (blue) of the maximum intensity. *Abbreviations*: Conventional = conventional radiation therapy; SBRT Z stereotactic body radiation therapy. (A color version of this figure is available at www.redjournal.org.)

Author Manuscript

Author Manuscript

Author Manuscript

Author Manuscript

Table 1

Patient characteristics

	Conventional RT cohort (n = 60)	SBRT cohort (n = 21)
SPECT scans available (n)		
Baseline	60	21
Mid-Tx	54	20
3Month Post-Tx	37	14
1Year Post-Tx	19	7
Age (y)		
Median	65	72
Range	39–85	53–83
Sex (n)		
Male	47	13
Female	13	8
Volume (lung GTV) (cm^3)		
Median	3842	3901
Range	1837–9540	1808–6489
Mean dose (lung GTV) (Gy)		
Median	13.1	7.4
Range	3.0–21.2	3.7–16.2

Abbreviations: 1Year Post-Tx = 1 year post-treatment; 3Month Post-Tx = 3 months post-treatment; GTV Z gross tumor volume; Mid-Tx = midcourse treatment; SBRT = stereotactic body radiation therapy; SPECT Z single-photon emission computed tomography.

Author Manuscript

Author Manuscript

Author Manuscript

Author Manuscript

Table 2

Population-level model parameters and standard deviations describing the expected dose-function response in well-perfused voxels at baseline (95% confidence intervals)

RT modality/time point	N	$E[\alpha_j] = \alpha$	$sd[\alpha_j]$	$E[\mu_j] = \mu$	$sd[\mu_j]$
Conventional RT/Mid-Tx	54	0.22 (0.16–0.27)	0.21 (0.17–0.26)	9.8 (4.1–15.5)	17.9 (13.9–23.1)
Conventional RTOMonth Post-Tx	37	0.72 (0.62–0.81)	0.28 (0.22–0.35)	18.2 (14.4–22.1)	10.9 (8.2–14.4)
Conventional RT/lYear Post-Tx	19	1.00 (0.80–1.21)	0.44 (0.28–0.69)	21.8 (8.9–34.7)	28.1 (19.8–40.0)
SBRT/Mid-Tx	20	0.24 (0.12–0.37)	0.27 (0.18–0.40)	45.0 (28.9–61.2)	35.3 (24.5–50.9)
SBRT/3Month Post-Tx	14	0.56 (0.46–0.66)	0.19 (0.13–0.27)	13.9 (4.4–23.3)	17.0 (10.8–26.7)
SBRT/1 Year Post-Tx	7	0.86 (0.56–1.15)	0.39 (0.23–0.67)	21.8 (18.3–25.3)	-

RT modality/time point	γ	σ	λ
Conventional RT/Mid-Tx	5.4 (4–0-6.8)	0.22 (0.19–0.26)	−0.11 (−0.13 to −0.08)
Conventional RTOMonth Post-Tx	9.6 (8.5–10.7)	0.32 (0.24–0.41)	−0.13 (−0.17 to −0.10)
Conventional RT/1Year Post-Tx	10.3 (8.7–12.0)	0.16 (0.10–0.25)	−0.03 (−0.10 to 0.03)
SBRT/Mid-Tx	14.0 (11.5–16.5)	0.10 (0.09–0.11)	−0.06 (−0.07 to −0.04)
SBRTOMonth Post-Tx	12.1 (9.9–14.4)	0.11 (0.10–0.13)	−0.01 (−0.04 to 0.01)
SBRT/1Year Post-Tx	20.4 (16.4–24.3)	0.12 (0.09–0.15)	0.03 (−0.03 to 0.08)

Abbreviations: 1Year Post-Tx = 1 year post-treatment; 3Month Post-Tx = 3 months post-treatment; Mid-Tx = midcourse treatment; SBRT Z stereotactic body radiation therapy.

Models with "-" listed in the sd[μ_j] column were unable to converge using patient-specific midpoints; thus, the same population-level midpoint was given to all patient in that cohort.

Author Manuscript

Author Manuscript

Author Manuscript

Author Manuscript

Table 3

Population-level model parameters and standard deviations describing the expected dose-function response stratified by functional categorization at baseline (95% confidence intervals)

RT modality/time point	E[αj] = α	sd[αj]	E[μj] = μ	sd[μj]	γ
Conventional RT/Mid-Tx	0.71 (−0.25 to 1.66)	−	46.6 (−102.6 to 195.8)	-	53.8 (−5.4 to 113.1)
Conventional RT/3Month Post-Tx	1.26 (1.19–1.33)	0.16 (0.13–0.21)	25.1 (20.6–29.6)	13.2 (10.3–16.9)	13.0 (11.9–14.1)
Conventional RT/1Year Post-Tx	1.23 (1.10–1.37)	0.23 (0.16–0.32)	17.9 (14.9–20.9)	-	15.4 (12.6–18.1)
SBRT/Mid-Tx	0.51 (0.43–0.59)	0.13 (0.09–0.18)	34.2 (19.1–49.3)		58.4 (41.5–75.2)
SBRT/3Month Post-Tx	0.86 (0.77–0.94)	0.16 (0.11–0.23)	14.6 (4.0–25.1)	19.8 (13.4–29.2)	13.3 (11.6–15.1)
SBRT/1Year Post-Tx	1.19 (1.02–1.36)	0.22 (0.13–0.38)	26.0 (14.1–37.9)	15.8 (9.1–27.2)	15.1 (13.3–16.9)
RT modality/time point	ω_1	ω_2	ω_3	σ	λ
Conventional RT/Mid-Tx	−0.90 (0.32 to −2.12)	−0.72 (0.26 to −1.69)	−0.45 (0.16 to −1.07)	0.51 (0.46–0.57)	−0.15 (−0.17 to −0.14)
Conventional RT/3Month Post-Tx	−1.17 (−1.13 to –1.22)	−0.89 (−0.85 to −0.93)	−0.53 (−0.49 to −0.56)	0.29 (0.25–0.32)	−0.10 (−0.12 to −0.08)
Conventional RT/1Year Post-Tx	−1.15 (−1.06 to −1.24)	−0.85 (−0.77 to −0.93)	−0.53 (−0.46 to −0.59)	0.44 (0.37–0.53)	−0.12 (−0.14 to −0.09)
SBRT/Mid-Tx	−0.57 (−0.50 to −0.63)	−0.43 (−0.38 to −0.49)	−0.29 (−0.25 to −0.33)	0.21 (0.20–0.22)	−0.09 (−0.10 to −0.08)
SBRT/3Month Post-Tx	−0.83 (−0.81 to −0.86)	−0.58 (−0.55 to −0.60)	−0.32 (−0.30 to −0.35)	0.17 (0.16–0.18)	−0.07 (−0.08 to −0.05)
SBRT/1Year Post-Tx	−1.04 (−0.98 to −1.09)	−0.69 (−0.64 to −0.73)	−0.38 (−0.33 to −0.43)	0.27 (0.25–0.30)	−0.13 (−0.14 to −0.11)

Abbreviations: 1Year Post-Tx = 1 year post-treatment; 3Month Post-Tx = 3 months post-treatment; GTV = gross tumor volume; Mid-Tx = midcourse treatment; SBRT = stereotactic body radiation therapy.

Models with "-" listed in the sd[μ_j] column were unable to converge using patient-specific midpoints; thus, the same population-level midpoint was given to all patient in that cohort. The number of patients contributing to each model is the same as shown in Table 2.